frontiers | Frontiers in Materials

TYPE Original Research
PUBLISHED 03 October 2023
DOI 10.3389/fmats.2023.1289250

OPEN ACCESS

EDITED BY
Shuomin Zhong,
Ningbo University, China

REVIEWED BY
Yunbo Li,
Southeast University, China
Cai Tong,
Zhejiang University, China
Yichao Liu,
Taiyuan University of Technology, China

*CORRESPONDENCE
Hao Wu,
12130001@zju.edu.cn
Huan Lu,
luhuan123@zju.edu.cn

RECEIVED 05 September 2023
ACCEPTED 22 September 2023
PUBLISHED 03 October 2023

CITATION
Zhu R, Chen T, Wang K, Wu H and Lu H (2023), Metasurface-enabled electromagnetic illusion with generic algorithm.
Front. Mater. 10:1289250.
doi: 10.3389/fmats.2023.1289250

Metasurface-enabled electromagnetic illusion with generic algorithm

Rongrong Zhu[1,2], Tianhang Chen[3], Kai Wang[2], Hao Wu[1]* and Huan Lu[2,4]*

[1]School of Information and Electrical Engineering, Hangzhou City University, Zhejiang, China, [2]Interdisciplinary Center for Quantum Information, State Key Laboratory of Extreme Photonics and Instrumentation, ZJU-Hangzhou Global Scientific and Technological Innovation Center, Zhejiang University, Hangzhou, China, [3]China Aeronautical Establishment, Beijing, China, [4]Key Laboratory of Advanced Micro/Nano Electronic Devices and Smart Systems of Zhejiang, Jinhua Institute of Zhejiang University, Zhejiang University, Jinhua, China

Electromagnetic cloak or illusion, which can interfere with device detection and provide superior self-protection capabilities for animals or humans, has received much attention. The proposal of transformation optics provides a generalized strategy for realizing electromagnetic illusion. However, the complex parameter composition causes a substantial computational cost, which is not conducive to practical applications. To overcome these challenges, we report an intelligent illusory metasurface optimized by a genetic algorithm, which not only presents predefined illusory effects but also reduces the parameter space in physics. By designing a high-performance tunable metasurface, a high-fidelity inverse design is performed in simulation. Near-field and far field results show that the metasurface can generate virtual targets in different scenarios and realize electromagnetic illusion. This work is helpful in facilitating the practical application of electromagnetic illusion strategies.

KEYWORDS

tunable metasurface, electromagnetic illusion, genetic algorithm, global optimization, inverse design

1 Introduction

Electromagnetic (EM) illusion technology is one of the most promising applications (Jiang et al., 2010; Jiang and Cui, 2011; Schittny et al., 2014; Xu et al., 2015; Yang et al., 2016; Huang et al., 2018; Cai et al., 2022; Liang et al., 2023), which can visually produce virtual objects that do not exist or transform an object into other forms, interfering with EM detection and ultimately achieving camouflage for active attack or passive defense. In traditional methods, optical illusions can be realized with the theory of transformation optics (Pendry et al., 2006; Schurig et al., 2006; Lai et al., 2009a; Lai et al., 2009b; Luo et al., 2009; Landy and Smith, 2013; Zheng et al., 2019), such as using complementary media to eliminate the original object and release the illusion of another object. However, this design is very complicated, and the extreme materials with anisotropy and inhomogeneity also make its practical application face a bottleneck. At the same time, a critical prerequisite for the realization of EM illusions is the acquisition of high-performance metamaterials/metasurfaces with the desired EM response.

Traditionally, this process of designing metasurfaces needs to be accomplished by time-consuming, inefficient, empirically guided numerical simulations or physically based

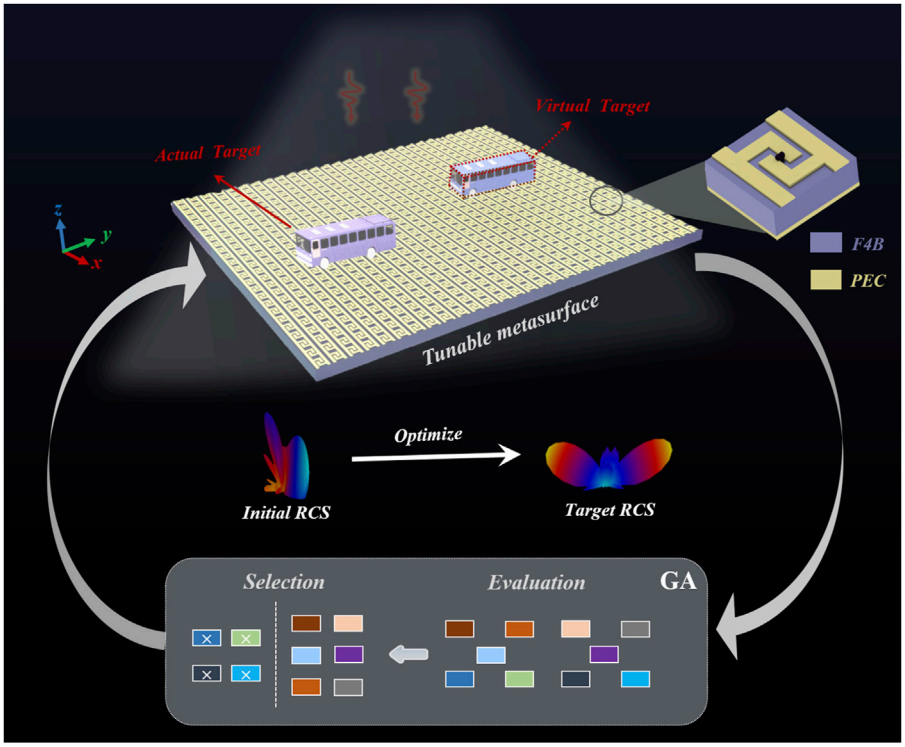

FIGURE 1
The conceptual diagram of GA-driven EM illusion.

methods; and theoretical methods will fail when the shape of the object is irregular (Chen et al., 2007; Li and Pendry, 2008; Hao et al., 2021; Shan et al., 2021; Hao et al., 2022). In recent years, intelligent optimization algorithms have emerged, strongly contributing to the study of metasurfaces (Goodfellow et al., 2016; Vaswani et al., 2017; Li et al., 2019; Qian et al., 2020; Shlezinger et al., 2021; Keeley et al., 2022; Ma et al., 2022; Shao et al., 2022; Lu et al., 2023; Zhong et al., 2023). Such as intelligent scattering and cloak (Qian et al., 2020), adaptive focusing (Lu et al., 2023), *etc*., which provide guidance for the inverse design of metasurfaces, and also provide the basis for realizing the EM illusion of false targets.

This study proposes an illusionary metasurface optimized using genetic algorithm (GA) (Lecun et al., 1998; Shakya, 2002; Pierro et al., 2004; Hinton et al., 2012; Lingaraj, 2016; Krizhevsky et al., 2017; Katoch et al., 2021) that can produce false targets in different scenarios. Firstly, the metasurface with high reflectivity and wide phase coverage is designed, and an adaptive regulation model of GA and metasurface is constructed. Different objective functions are selected according to the requirements in different environments, and the tunable metasurface satisfying the predefined objectives is reverse-designed after global optimization and iteration of the algorithm. Ultimately, illusory scattering that produces false vehicle targets is achieved using the metasurface in both the absence of objects and the presence of a single object. Despite the operating frequency being 5 GHz, the optimization method has no restriction on the frequency, and false scattering can be achieved at other arbitrary frequencies by simply modifying the appropriate objective function. This work eliminates the need for theoretical computation of complex parameters and allows iterative generation of spurious scattering given only the optimization objective. It has a wide range of promising applications in various aspects, such as metasurface inverse design and intelligent tuning.

2 Methods

Figure 1 illustrates the conceptual diagram of an EM illusion using the tunable metasurface to generate the virtual target. The intelligent metasurface consists of a series of tunable unit cells (as shown in the inset at the top right), and it is independently tunable in one-dimensional direction (*y*-direction) for each cell to produce a rich EM response. When an object exists on the metasurface (actual target), initial radar cross section (RCS) is generated under the effect of EM waves. The observer can recognize the target by judging the approximate shape of the object based on the RCS. If other types of far-field RCS can be generated, the detection device will be interfered with to realize EM illusion. As shown in Figure 1, using the target RCS as the objective function, after the global optimization of the GA and the modulation of the metasurface, the system finally produces the RCS that is generated only when two targets exist, i.e., the virtual target is generated.

A high-performance tunable reflection unit cell is designed to generate the false targets. Figure 2A shows the designed structure, consisting of a dielectric substrate and a metal with a relative permittivity $\varepsilon_r = 2.65$, a loss angle tangent of 0.002, a thickness of 2.5 mm, and a size of 10×10 mm^2. The backside of this structure is an all-reflective metal layer, which ensures a high reflectivity of the incident EM wave. The metal on the front side of the unit cell is

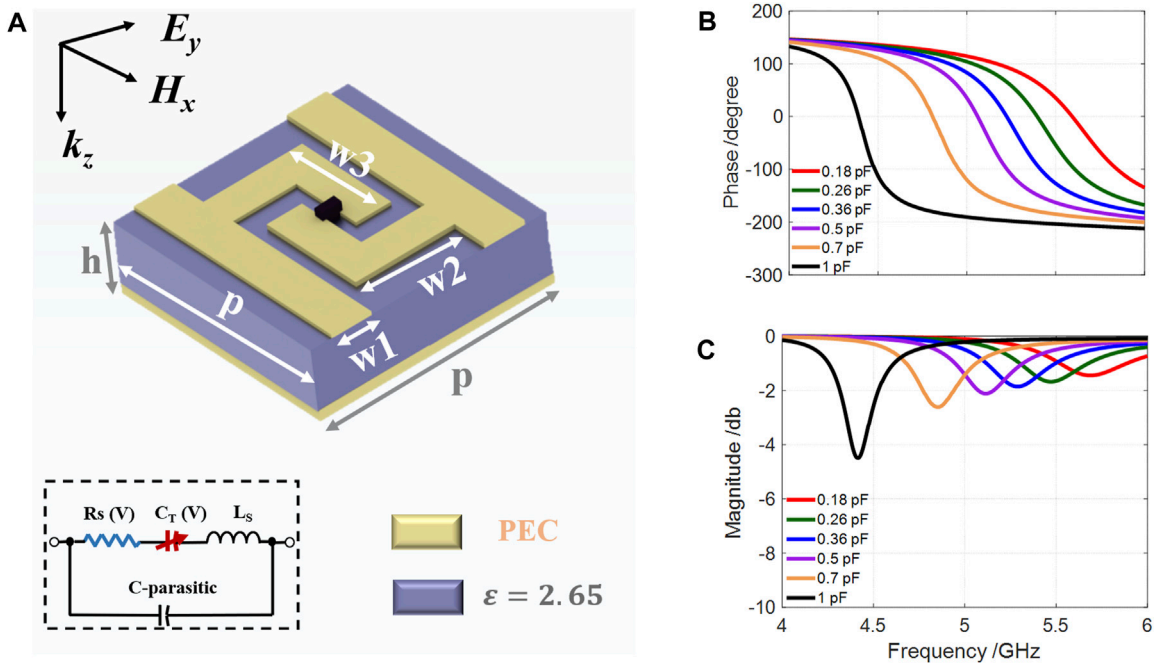

FIGURE 2
The unit cell and S-parameters. **(A)** Schematic diagram of the unit cell, where $p = 10\,mm$, $w1 = 1.5\,mm$, $w2 = 4.2\,mm$, $w3 = 4.5\,mm$, and $h = 2.5\,mm$. **(B)** The phase response of the unit cell. **(C)** The magnitude response of the unit cell.

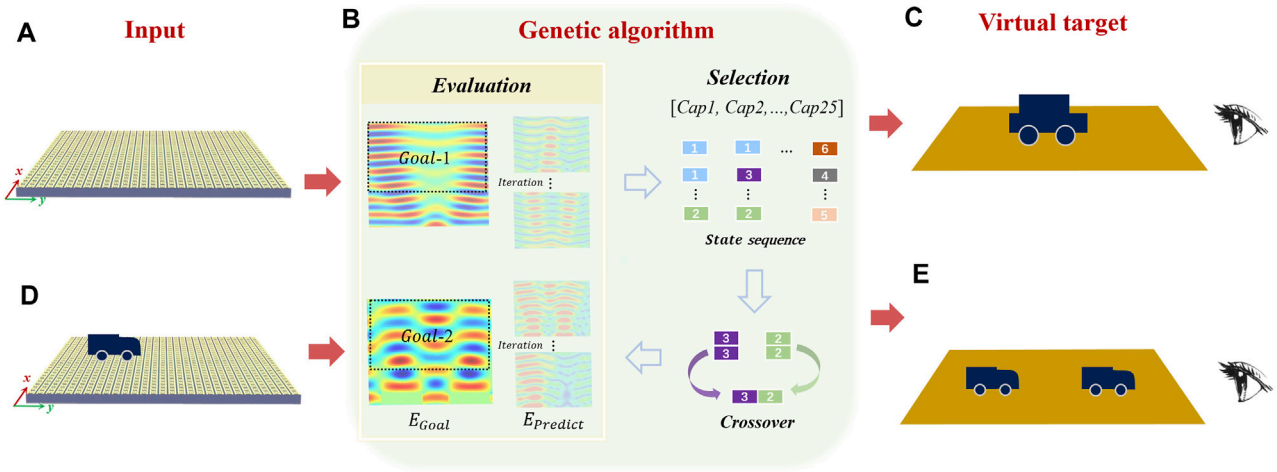

FIGURE 3
The process for generating false targets in different scenarios using GA and metasurface. **(A)** Input data for the first scenario. **(B)** Genetic algorithm process. **(C)** The first illusion scene. **(D)** Input data or the second scenario. **(E)** The second illusion scene.

centrosymmetric in which a varactor diode is embedded in the middle. The diode model is a MAVR-000120-14110P varactor manufactured by MACOM, which has an adjustable capacitance between 0.14 pF and 1.1 pF with a parasitic resistance of 2.5 Ω. The equivalent circuit diagram of the capacitive diode is shown in the inset portion of Figure 2A. In the actual simulation, the RC model is used as the equivalent circuit, and the characteristics of the diode can be changed by adjusting the capacitance. We analyze the S-parameters using the CST2021 in the frequency domain mode. For simulation, both the x and y directions are set as unit cell boundaries, the electric field along the y direction, and the magnetic field along the x direction.

The S-parameter characteristics are shown in Figures 2B, C. The horizontal coordinate represents the frequency change. It can be seen that the reflection phase varies continuously up to 330° at $f = 5\,GHz$ (Figure 2B), and the reflection amplitude is better

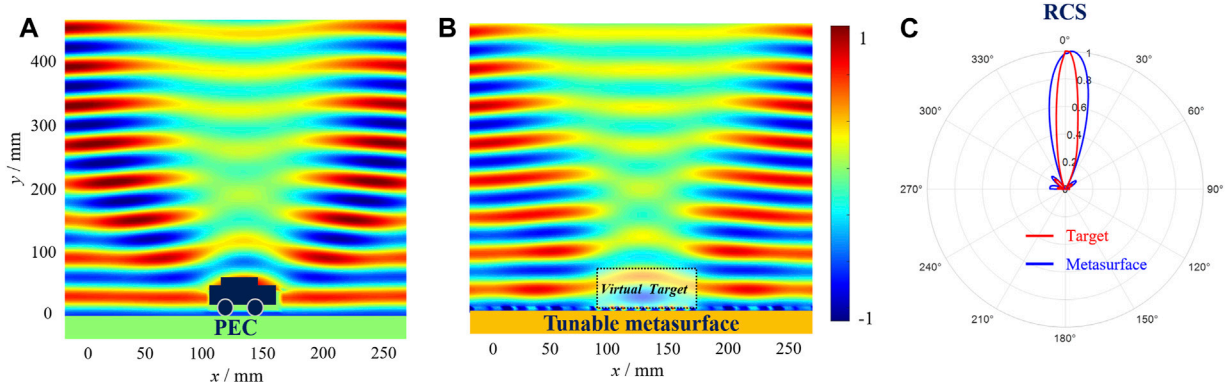

FIGURE 4
Metasurface generates the false vehicle target. **(A)** Scattering of the object. **(B)** Scattering of the metasurface. **(C)** The results of the RCS.

than −2 dB (Figure 2C). The unit cell can achieve continuous phase by adjustment the capacitance. In order to increase the speed of the global optimization, we chose six capacitors as feature with capacitance values of 0.18, 0.26, 0.36, 0.5, 0.7, and 1 pF, respectively. The corresponding phases are 130°, 100°, 70°, 40°, −110°, and −200°, respectively. They are also used for the subsequent iterations of the algorithm. Even if the phase response of a single structure does not reach 360°, rich EM modulation can be realized by global tuning of the metasurface.

The virtual target is then generated using GA and the metasurface, the progress is illustrated in Figure 3. The metasurface is composed of a set of tunable unit cells, the state is independently along the y-direction, and it is periodically arranged along the x-direction. The size of the metasurface is $200mm \times 250mm$, as shown in Figure 3A. Figure 3B shows the iterative flow of the GA. In general, the algorithm includes evaluation, selection, and crossover/mutation. The "evaluation" means the loss between predicted and actual results, also known as the objective function; the "selection" is to select different state sequences, and the "crossover" is an update strategy. Defining the loss function using mean absolute error (MAE):

$$MAE = \frac{1}{m}\sum_{i=1}^{m}\left|E_{Theory} - E_{Test}\right| \tag{1}$$

where E_{Theory} is the target electric field, and the E_{Test} is the electric field generated during the iteration. If the iteration termination condition is not satisfied at the moment t, the algorithm re-selects the state sequence (i.e., capacitance $[Cap1, Cap2, ..., Cap25]$) at the moment $t+1$ according to the loss function. After that, the metasurface state changes and will generate the new electric field. The GA re-judges the error at this time, and terminates the iteration if the condition is satisfied. Otherwise, the next update is performed.

In the first case, we take the electric field generated by the metasurface as the input (Figure 3A) and take the single-vehicle scattering data as the target (Goal-1 in Figure 3B). After global optimization by the GA, we can eventually generate the scattering field similar to one vehicle target, thus confusing the observer, as shown in Figure 3C.

In the second case, the electric field generated by the metasurface and the vehicle together is used as the input (Figure 3D). Taking it as the goal data (Goal-2 of Figure 3B), the system can generate the electric field that similar to two vehicle targets after global optimization, thus creating a false target (as shown in Figure 3E). After being driven and guided by the GA, the various virtual target can be generated in different scenarios, interfering with the detection and realizing the EM illusion.

The results of generating one false vehicle target are shown in Figure 4. Figure 4A shows the results of the real part of the electric field of the vehicle model on a metal ground, where it can be seen that there is strong backward scattering. The vehicle model has a height of about 60 mm and a length of about 70 mm. The electric field is used as the target data. Using GA to optimize and adjust the metasurface, and the final iteration electric field is shown in Figure 4B. In Figure 4, the horizontal coordinate x denotes the length of the metasurface, and the vertical coordinate y denotes the distance from the metasurface, and all data are normalized. A comparison of Figs a and b shows that there is a high similarity, which means the metasurface produces a false target that approximates the vehicle model. The MAE loss is 0.15.

Figure 4C shows the comparison results of the far-field RCS, where the red solid line is the RCS produced by the target (Figure 4A) and the blue solid line is the RCS produced by the metasurface (Figure 4B). The RCS was defined as:

$$\sigma = 2\pi\rho\left|H_y^o - H_y^g\right|^2 \tag{2}$$

where H_y^o and H_y^g are the electric field in the object and background cases respectively. Calculating the correlation coefficient $r(E_{Theory}, E_{Test})$ for Figure 4C, which is defined as:

$$r\left(E_{Theory}, E_{Test}\right) = \frac{C\left(E_{Theory}, E_{Test}\right)}{\sqrt{Var\left[E_{Theory}\right]Var\left[E_{Test}\right]}} \tag{3}$$

$$\begin{aligned} C\left(E_{Theory}, E_{Test}\right) &= \mathbf{E}\left[\left(E_{Theory} - \mathbf{E}\left[E_{Theory}\right]\right)\left(E_{Test} - \mathbf{E}\left[E_{Test}\right]\right)\right] \\ &= \mathbf{E}\left[E_{Theory}E_{Test}\right] - 2\mathbf{E}\left[E_{Test}\right]\mathbf{E}\left[E_{Theory}\right] + \mathbf{E}\left[E_{Theory}\right]\mathbf{E}\left[E_{Test}\right] \\ &= \mathbf{E}\left[E_{Theory}E_{Test}\right] - \mathbf{E}\left[E_{Theory}\right]\mathbf{E}\left[E_{Test}\right] \end{aligned} \tag{4}$$

where $C(E_{Theory}, E_{Test})$ is the covariance of E_{Theory} and E_{Test}, $Var[E_{Theory}]$ is the variance of E_{Theory}, and $Var[E_{Test}]$ is the variance of E_{Test}. $\mathbf{E}$ is the mathematical expectation. The correlation between the two curves in Figure 4 was calculated to be 96.2%. Thus, the

10.3389/fmats.2023.1289250

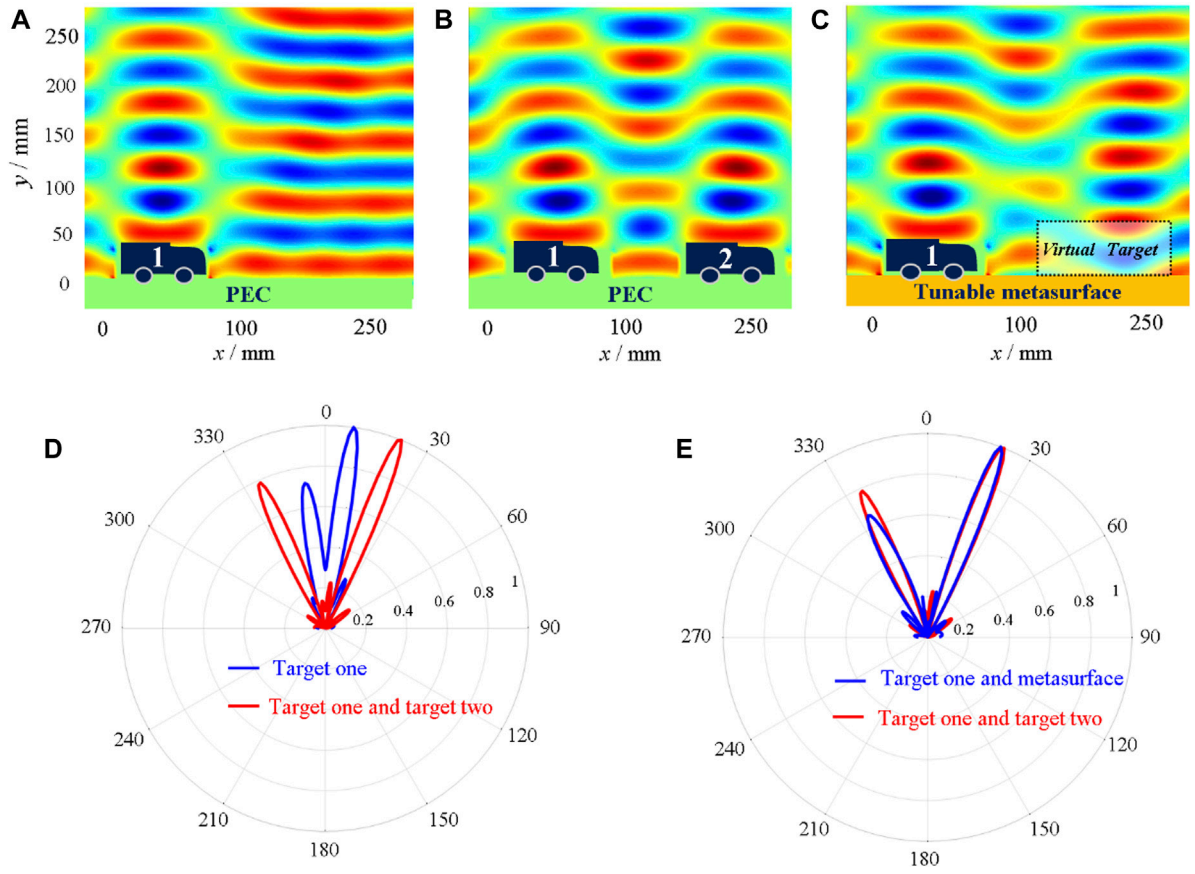

FIGURE 5
Metasurface generates the false vehicle target in another scenario. **(A)** Scattering of the target one. **(B)** Scattering of targets one and two. **(C)** Scattering from metasurface and target one. **(D,E)** Comparison of RCS in different scenarios.

ability of the metasurface to generate false targets is demonstrated in both the near and far fields.

Figure 5 shows the results of the metasurface generating a virtual target in another scenario. In Figure 5A, a vehicle target made of PEC is placed above a metallic ground and generates scattering, labeling the object as target one. In Figure 5, the horizontal coordinate x denotes the length of the metasurface and the vertical coordinate y denotes the distance from the metasurface. Two identical vehicles (target one and target two) were placed above the PEC, and their near-field scattering is shown in Figure 5B. The effect of the metal object results in inhomogeneity across the real part of the electric field. Using the data in Figure 5B as the goal function, and the final iteration electric field is shown in Figure 5C. The comparative results of Figures 5B, C reveal the consistency of the electric field, at which point the MAE loss is 0.18.

Figures 5D, E show the far-field RCS results. In Figure 5D, the blue solid line is the RCS generated by target one (i.e., Figure 5A). The red solid line is the RCS generated by target one and target two together (i.e., Figure 5B), and the correlation of the curves is only 20%. After global optimization, the far-field RCS generated by the metasurface and target one has a high similarity with the two targets, as shown in Figure 5E, and the correlation coefficient is 97.3%.

3 Conclusion

In conclusion, we implement a joint GA and metasurface to realize an EM phantom for false target generation, and this joint modulation model is validated to be effective in different scenarios. High-performance and reliable tunable reflective hypersurface structures are designed, which can achieve a continuous phase change of about 330° at the operating frequency while the amplitude is better than −2 db. The metasurface arrays designed with the assistance of genetic algorithms can generate scattering from vehicle targets in both scenarios with no objects or in the presence of a single object, and both near-field and far-field data validate the effectiveness of the simulations. Compared to traditional deep learning algorithms, GA can achieve global optimization with unlabeled data and explore more parsing solutions to the problem. In scenarios with more targets, only the optimization objective function is modified to achieve false scattering for different scenarios. This work provides new ideas for EM metasurface inverse design and can be used to decode richer structures.

Data availability statement

Data can be obtained from the corresponding author (HL).

Author contributions

RZ: Investigation, Validation, Writing–original draft. TC: Writing–review and editing, Supervision. KW: Writing–review and editing, Supervision. HW: Investigation, Methodology, Supervision, Writing–review and editing. HL: Conceptualization, Methodology, Writing–review and editing.

Funding

The authors declare financial support was received for the research, authorship, and/or publication of this article. This work was sponsored by the Natural Science Foundation of Zhejiang Province under Grant No. LQ21F050002.

Conflict of interest

The authors declare that the research was conducted in the absence of any commercial or financial relationships that could be construed as a potential conflict of interest.

The reviewer CT declared a shared affiliation with the author HL to the handling editor at time of review.

Publisher's note

References

Cai, T., Zheng, B., Lou, J., Shen, L., Yang, Y., Tang, S., et al. (2022). Experimental realization of a superdispersion-enabled ultrabroadband terahertz cloak. *Adv. Mat.* 34 (38), 2205053. doi:10.1002/adma.202205053

Chen, H., Wu, B.-I., Zhang, B., and Kong, J. A. (2007). Electromagnetic wave interactions with a metamaterial cloak. *Phys. Rev. Lett.* 99 (6), 063903. doi:10.1103/physrevlett.99.063903

Goodfellow, I., Bengio, Y., and Courville, A. (2016). *Deep learning*. Cambridge, MA, USA, MIT Press.

Hao, H., Ran, X., Tang, Y., Zheng, S., and Ruan, W. (2021). A single-layer focusing metasurface bassed on induced magnetism. *Prog. Electromagn. Res.* 172, 77–88. doi:10.2528/pier21111601

Hao, H., Tang, Y., Zheng, S., Ran, X., and Ruan, W. (2022). Design of circular polarization multiplexing beam splitter based on transmission metasurface. *Prog. Electromagn. Res. M.* 109, 125–136. doi:10.2528/pierm22010408

Hinton, G., Deng, L., Yu, D., Dahl, G. E., Mohamed, A., Jaitly, N., et al. (2012). Deep neural networks for acoustic modeling in speech recognition:the shared views of four research groups. *IEEE Signal Proc. Mag.* 29 (6), 82–97. doi:10.1109/msp.2012.2205597

Huang, C., Yang, J., Wu, X., Song, J., Pu, M., Wang, C., et al. (2018). Reconfigurable metasurface cloak for dynamical electromagnetic illusions. *ACS Photonics* 5 (5), 1718–1725. doi:10.1021/acsphotonics.7b01114

Jiang, W. X., and Cui, T. J. (2011). Radar illusion via metamaterials. *Phys. Rev. E* 83 (2), 026601. doi:10.1103/physreve.83.026601

Jiang, W. X., Ma, H. F., Cheng, Q., and Cui, T. J. (2010). Illusion media:generating virtual objects using realizable metamaterials. *Appl. Phys. Lett.* 96 (12), 121910. doi:10.1063/1.3371716

Katoch, S., Chauhan, S. S., and Kumar, V. (2021). A review on genetic algorithm:past, present, and future. *Multimed. Tools Appl.* 80 (5), 8091–8126. doi:10.1007/s11042-020-10139-6

Keeley, E., Joe, L., Colin, G., and Ian, J. (2022). Machine-learning-enabled recovery of prior information from experimental breast microwave imaging data. *Prog. Electromagn. Res.* 175, 1–11. doi:10.2528/pier22051601

Krizhevsky, A., Sutskever, I., and Hinton, G. E. (2017). ImageNet classification with deep convolutional neural networks. *Commun. ACM* 60 (6), 84–90. doi:10.1145/3065386

Lai, Y., Chen, H., Zhang, Z.-Q., and Chan, C. T. (2009b). Complementary media invisibility cloak that cloaks objects at a distance outside the cloaking shell. *Phys. Rev. Lett.* 102 (9), 093901. doi:10.1103/physrevlett.102.093901

Lai, Y., Ng, J., Chen, H., Han, D., Xiao, J., Zhang, Z.-Q., et al. (2009a). Illusion optics: the optical transformation of an object into another object. *Phys. Rev. Lett.* 102 (25), 253902. doi:10.1103/physrevlett.102.253902

Landy, N., and Smith, D. R. (2013). A full-parameter unidirectional metamaterial cloak for microwaves. *Nat. Mat.* 12 (1), 25–28. doi:10.1038/nmat3476

Lecun, Y., Bottou, L., Bengio, Y., and Haffner, P. (1998). Gradient-based learning applied to document recognition. *Proc. IEEE* 86 (11), 2278–2324. doi:10.1109/5.726791

Li, J., and Pendry, J. B. (2008). Hiding under the carpet: A new strategy for cloaking. *Phys. Rev. Lett.* 101 (20), 203901. doi:10.1103/physrevlett.101.203901

Li, L., Shuang, Y., Ma, Q., Li, H., Zhao, H., Wei, M., et al. (2019). Intelligent metasurface imager and recognizer. *Light. Sci. Appl.* 8 (1), 97. doi:10.1038/s41377-019-0209-z

Liang, Q., Li, Z., Xu, J., Duan, Y., Yang, Z., and Li, D. (2023). A 4D-printed electromagnetic cloaking and illusion function convertible metasurface. *Adv. Mat. Technol.* 2202020. doi:10.1002/admt.202202020

Lingaraj, H. (2016). A study on genetic algorithm and its applications. *Int. J. Comput. Sci. Eng.* 4, 139–143.

Lu, H., Zhao, J., Zheng, B., Qian, C., Cai, T., Li, E., et al. (2023). Eye accommodation-inspired neuro-metasurface focusing. *Nat. Commun.* 14 (1), 3301. doi:10.1038/s41467-023-39070-8

Luo, Y., Zhang, J., Chen, H., Ran, L., Wu, B.-I., and Kong, J. A. (2009). A rigorous analysis of plane-transformed invisibility cloaks. *IEEE Trans. Antenn. Propag.* 57 (12), 3926–3933. doi:10.1109/tap.2009.2027824

Ma, W., Xu, Y., Xiong, B., Deng, L., Peng, R. W., Wang, M., et al. (2022). Pushing the limits of functionality-multiplexing capability in metasurface design based on statistical machine learning. *Adv. Mater* 34 (16), 2110022. doi:10.1002/adma.202110022

Pendry, J. B., Schurig, D., and Smith, D. R. (2006). Controlling electromagnetic fields. *Science* 312 (5781), 1780–1782. doi:10.1126/science.1125907

Pierro, D.-F., Khu, S.-T., and Djordjevi, S. (2004). *A new genetic algorithm to solve effectively highly multi- objective problems: POGA, report nr*. Center for WaterSystems, University of Exeter., London, UK ,

Qian, C., Zheng, B., Shen, Y., Jing, L., Li, E., Shen, L., et al. (2020). Deep-learning-enabled self-adaptive microwave cloak without human intervention. *Nat. Photonics* 14 (6), 383–390. doi:10.1038/s41566-020-0604-2

Schittny, R., Kadic, M., Bückmann, T., and Wegener, M. (2014). Invisibility cloaking in a diffusive light scattering medium. *Science* 345 (6195), 427–429. doi:10.1126/science.1254524

Schurig, D., Mock, J. J., Justice, B. J., Cummer, S. A., Pendry, J. B., Starr, A. F., et al. (2006). Metamaterial electromagnetic cloak at microwave frequencies. *Science* 314 (5801), 977–980. doi:10.1126/science.1133628

Shakya, S. K. (October 2002). "Probabilistic model building genetic algorithm (pmbga): A survey," in Proceedings of the 7th international conference, granada, Spain.

Shan, T., Li, M., Xu, S., and Yang, F. (2021). Phase synthesis of beam-scanning reflectarray antenna based on deep learning technique. *Prog. Electromagn. Res.* 172, 41–49. doi:10.2528/pier21091307

Shao, S., Fan, M., Yu, C., Li, Y., Xu, X., Wang, H., et al. (2022). Machine learning-assisted sensing techniques for integrated communications and sensing in WLANs:current status and future directions. *Prog. Electromagn. Res.* 175, 45–79. doi:10.2528/pier22042903

Shlezinger, N., Alexandropoulos, G. C., Imani, M. F., Eldar, Y. C., and Smith, D. R. (2021). Dynamic metasurface antennas for 6G extreme massive MIMO communications. *IEEE Wirel. Commun.* 28 (2), 106–113. doi:10.1109/mwc.001.2000267

Vaswani, A., Shazeer, N., Parmar, N., Uszkoreit, J., Jones, L., Gomez, A. N., et al. (January 2017). "Attention is all you need," in Proceedings of the neural information processing systems (Long Beach, CA, USA:).

Xu, S., Xu, H., Gao, H., Jiang, Y., Yu, F., Joannopoulos, J. D., et al. (2015). Broadband surface-wave transformation cloak. *Proc. Nat. Acad. Sci.* 112 (25), 7635–7638. doi:10.1073/pnas.1508777112

Yang, Y., Jing, L., Zheng, B., Hao, R., Yin, W., Li, E., et al. (2016). Full-polarization 3D metasurface cloak with preserved amplitude and phase. *Adv. Mat.* 28 (32), 6866–6871. doi:10.1002/adma.201600625

Zheng, B., Yang, Y., Shao, Z., Yan, Q., Shen, N.-H., Shen, L., et al. (2019). Experimental realization of an extreme-parameter omnidirectional cloak. *Research* 2019 (8282641), 8282641. doi:10.34133/2019/8282641

Zhong, S., Wang, X., and Tretyakov, S. (2023). Coherent control of wave beams via unidirectional evanescent modes excitation. *Adv. Funct. Mater*, 15, 2304300. doi:10.1002/adfm.202304300